J. Biochem. **139**, 329–338 (2006)
doi:10.1093/jb/mvj038

Lymphocyte Toxicity of Prion Fragments

Jayaraman Murali* and Rajadas Jayakumar†
Bioorganic and Neurochemistry Laboratory, Central Leather Research Institute, Adyar, Chennai–600 020, India

Received April 23, 2005; accepted August 29, 2005

Prion protein fragments that are extracted from the brains of patients with Gerstmann-Straussler-Scheinker disease are known to have stimulating action on circulating leukocytes. In particular, the amyloidogenic hydrophobic prion peptide HuPrP (113–127) AGAAAAGAVVGGLGG has been reported to be associated with significant cellular toxicity. In this paper we show that the self assembled form of HuPrP (113–127) and its valine rich domains viz. GAVVGGLG [HuPrP (119–126)] and VVGGLGG [HuPrP (121–127)] are toxic to peripheral lymphocytes. To explore the cytotoxic mechanism of these fragments, we studied 3-(4,5-dimethylthiazol-2yl)-2–5-diphenyltetrazolium bromide (MTT) reduction, reactive oxygen species (ROS) generation, calcium influx and raft sequestration of' peptide treated lymphocytes. Langmuir monolayer studies on these peptides showed a maximum lipid perturbing property of HuPrP (121–127) as compared to the other two fragments. MTT reduction assays on lymphocytes treated with peptides indicated that the prion peptide fibrils are relatively more toxic than freshly solubilized peptide preparations. Lymphocytes treated with HuPrP (121–127), HuPrP (113–127) and HuPrP (119–126) fibrils underwent 60%, 30% and 40% cell death, respectively. Aβ(1–42), HuPrP (119–126) and HuPrP (121–127) fibrils caused 4 fold increases in intracellular ROS as compared with control cells. However, HuPrP (113–127) fibrils lacked such a significant ROS generating activity, indicating that a subtle difference in sequence leads to a difference in the toxic mechanism in the cell. HuPrP (119–126) and HuPrP (121–127) fibrils also produced maximum raft sequestration and calcium influx. Taken together, these data suggest that the assemblage of prion fragments has significant toxic activity on peripheral lymphocytes, a finding with implications for controlling reactive lymphocytes in prion infected subjects.

Key words: amyloid fibril, calcium influx, oxidative stress, prion, raft sequestration, segmental toxicity.

Prion diseases, also termed Transmissible Spongiform Encephalopathies (TSEs), are amyloid based chronic neurodegenerative disorders that affect humans and animals. TSEs, including Bovine Spongiform Encephalopathy, sheep scrapie, and Creutzfeldt-Jakob Disease (vCJD) in humans, are transmitted by peripheral exposure. After an infective particle enters the gut, it is sequestered in the spleen before neuroinvasion (*1–4*). Prions, in the infective form, are composed of a protofibrillar (PF) structure, in which some of them are amenable to epitopic processing (*5*). Several groups have recently studied the possibility of cellular degradation as a result of PrP^{Sc} exposure (*6–8*). This is especially true of macrophages, which are involved in the degradation of PrP^{Sc} into peptide fragments (*9*, *10*). Notably, vaccination with self-PrP peptides has been shown to reduce PrP^{Sc} formation in transplanted scrapie-infected neuroblastma cells in mouse models, indicating that the smaller fragments play a crucial role in the infection progression of the prion particles (*11*).

Furthermore, receptor binding and stimulation of pro-inflammatory responses of the toxic prion fragment PrP (106–126) have been observed in mononuclear phagocytes (*12*). The prion fragments PrP (89–106), PrP (106–114) and PrP (127–147) peptides have been reported to stimulate human T lymphocytes (*13*). Propagation of blood prions into the central nervous system (*i.e.*, neuroinvasion) requires the depletion of active lymphatic cells, which are sensitive to peptide epitopes (*2*, *14*). Hence, the toxic effects of partially metabolized prion fragments by selective lymphocyte populations are essential for prion infectivity. In our earlier work, we demonstrated the conformational polymorphism among short prion fragments, namely, PrP (113–127), PrP (119–126) and PrP (121–127) (*15*, *16*). These shorter peptides have been shown to form amyloid like assemblages *in vitro*, and they elicit neurotoxic activity towards primary cultures of rat astrocytes (*15–17*). PrP (106–126) consists of an N-terminal polar head (KTNMKHM) followed by a long hydrophobic tail (AGAAAAGAVVGGLG), and readily forms neurotoxic amyloid like fibrils (*18–22*). Previous studies identified a smaller region of the prion, namely PrP (106–126), as the most toxic component of the entire protein (*19*, *23*). These regions under normal conditions, self assemble into protease resistant toxic aggregates without the addition of infectious protein seeding. Notably, this assembly induces

*Present address: Graduate School of Medicine, University of Tennessee, 1924 Alcoa Highway, Knoxville, TN 37920, USA.
†To whom correspondence should be addressed. PABX: +91-44-24911386 (Ext. 324), Fax: +91-44–24911589, E-mail: karkuvi77@yahoo.co.uk

a phenotypic expression similar to that of full length PrP^{Sc} (*24*). The toxic mechanism of these peptides also resembles the full length PrP^{Sc}. However, the toxic function and phenotypic alteration require the neuronal expression of PrP^{C} and microglial participation (*25–27*). It is quite likely that antioxidant depletion produced by microglial cells could be the causative agent of the neuronal death by PrP (106–126), likely caused by the induction of calcium influx through L-type channels and NMDA receptors (*28*). Several groups have studied the structural details of this sequence and found that a palindrome sequence corresponding to amino-acid residues 113–126 adopts amyloid structures, similar to other toxic amyloid assemblage (*15*, *20–22*). Although the lymphatic system has been shown to be important in the pathogenesis of prion diseases in animal models, the mechanisms by which lymphocytes participate in the propagation of PrP^{Sc} are not known. The current work was designed to ascertain the toxic effects of PrP fragments on human peripheral blood lymphocytes. The results of the present investigation indicate that the assemblages of PrP fragments induce cell death in a coordinated mode through sequestration of lipid rafts, the generation of reactive oxygen species, and the modulation in calcium influx.

MATERIALS AND METHODS

Materials Used—The prion peptide sequences used in this study are AGAAAAGAVVGGLGG, GAVVGGLG, VVGGLGG, which correspond to human prion protein residues HuPrP (113–127), HuPrP (119–126) and HuPrP (121–127), respectively. These peptides were synthesized by a solid phase method using the *t*-butyloxy carbonyl group (Boc) as the protective group for the N-termini. The carboxylic ends were activated by the addition of 1-hydroxy benzotriazole (HOBt) and *N*,*N*-dicyclohexylcarbodiimide (*29*). The final peptide was cleaved and deprotected from the 4-methylbenzhydrylamine (MBHA) resin simultaneously with trifluoromethanesulfonic acid/thioanisole/ethanedithiol/trifluoroacetic acid (1:1:1:7) and precipitated with cold ether. The purity and composition were determined by amino acid analysis and identified by MALDI-TOF MS analysis. The Aβ(1–42) peptide was obtained from Biosource International (Camarillo, CA). Synthesis, characterization and details of the conformations of prion peptides in solution are published elsewhere (*15–17*). The fluorescence probes Fura–2 AM, Dichloro dihydrofluorescein diacetate (H_2DCF-DA) and the tetrazolium dye, 3-(4,5-Dimethylthiazol-2yl)-2–5-diphenyltetrazolium bromide (MTT) were obtained from Sigma (St. Louis, MO). Phosphatidyl choline-dipalmitoyl and cholesterol were obtained from Avanti Polar Lipids, Inc. (Alabaster, AL).

Langmuir–Blodgett Film Studies. Surface Pressure-Area Isotherm Studies—The Wilhelmy plate method was used to study the surface activity of prion peptide fragments. The Langmuir-Blodgett films of the PrP peptide were prepared, as described earlier (*15*), by spreading 50 μl of sample in a mixture of chloroform/methanol (90:10, v/v) containing prion peptide on 10% acetonitrile in 10 mM phosphate buffer, pH 7.4, prepared in purified water (Milli Q system, Millipore Ltd.). The peptide concentration of the spreading solution was 1 mg/ml. After 15 min of spreading, the gaseous monolayer was continuously compressed. Similarly, the experiments were also carried out in the presence of a lipid monolayer formed by spreading a mixture of phosphatidyl choline–dipalmitoyl and cholesterol. The compression was maintained at the rate of 250 nm/s during the isotherm measurement. Teflon-Coated troughs, with a coprocessor controlled film balance (NIMA trough 611) and a precision of 0.01 mN/m, were used for surface pressure measurements. The measurements of surface pressure (π) – Area (*A*) isotherms were recorded several times to check their reproducibility.

The number of peptide layers in the film was evaluated by the following equation:

$$\text{Numberoflayers}[N] = [A]/A_0$$

where [*A*] is the average area per residue for (β-sheet forming peptide and A_0 is area per residue obtained from the measurements (*30*).

Insertion Studies of Prion Peptides Using Membrane Monolayers—Lipid monolayers were prepared by spreading a 2:1 mixture of phosphatidyl choline–dipalmitoyl and cholesterol. Typically, 50 μg of lipid was used for monolayer formation, and, thereby, the change in the final surface area was restricted to 20–25% of the maximum surface area available. This allowed us to measure the expansion of area followed by the insertion of the peptide. Lipid monolayers were compressed using a Langmuir film balance (NIMA Technology, Coventry, UK) with a surface pressure feedback system to measure the area per lipid molecule (*i.e.*, monolayer expansion or contraction) at constant surface pressure. The surface pressures were kept between 17–22 mNm^{-1} to offer an area of 75 $Å^2$ per molecule of pure lipid. After the lipid monolayer was constructed, the peptides were added to the subphase to provide a final subphase concentration of 5 μM, and the resulting area change (Δ*A*) was recorded over a period of time. A pure water isotherm was recorded before each experiment to confirm the absence of residual surface impurities. The initial surface pressure was maintained through programmed control of barrier movements, and any change in surface area was measured. The peptide surface spreading property in mixed lipid–peptide monolayers was obtained using the surface phase rule as described in the literature (*31*, *32*).

Separation of Lymphocytes—Fresh blood from healthy volunteers was gently layered on Ficoll solution (9.56 g Ficoll, 20 ml pure iodamide, 130 ml dH_2O) (Amersham Biosciences, Sweden), and the samples were centrifuged at 1,800 rpm for 20 min. The lymphocyte-containing bands were separated and rinsed three times with phosphate buffered saline (PBS) as reported earlier (*33*). Cell concentration was estimated using Neubar's chamber. Freshly prepared lymphocytes in PBS were used for calcium measurements. Cell viability, as assessed by Trypan blue dye exclusion, was greater than 97%.

MTT Reduction Assay—The reduction of 3-(4,5-Dimethylthiazol-2yl)-2–5-diphenyltetrazolium bromide (MTT) by lymphocytes was assayed as described (*4*). Briefly, prion peptides were pre-incubated at a concentration of 250 μM in 20 mM HEPES, pH 7.4, at 37°C for one and three days, then diluted in 100 μl of lymphocyte culture medium to yield final peptide concentrations of

25 and 60 μM of HuPrP (113–127), HuPrP (119–126) and HuPrP (121–127) peptides. Freshly solubilised prion peptides were also incubated with lymphocytes. Aβ (1–42) fibrils were used as a positive control. MTT was diluted to 0.5 mg/ml in Hank's solution (Gibco) and added to the culture for 1 h at 37°C. The MTT formazon product was released from the cells by the addition of dimethyl sulfoxide, and the amount was measured by absorption at 570 nm.

Assessment of Free Radicals in Lymphocytes—To assay the prion peptide fibril–induced alteration of intracellular H_2O_2, as a consequence of catalase or Cu/Zn-SOD overexpression, the oxidation of the dye 2,7-dichlorodihydro fluorescein diacetate (H_2DCF-DA) was monitored by using a Cary Bio-50 spectrofluorimeter. A stock solution of 1 mM DCFH-DA in absolute ethanol was prepared and kept in the dark. From the stock, 10 μl of DCFH-DA was added to cells. The samples were excited at 485 nm and the fluorescence intensity was measured at 530 nm. Initial fluorescence values (time 0) were found to differ from each other by less than 5%. The results were expressed as the percentage increase in fluorescence calculated using the following equation:

$$[(F_{t30} - F_{t0})/F_{t0} \times 100]$$

Where F_{t0} and F_{t30} are the fluorescence intensities at 0 and 30 min, respectively. This dye allows the determination of intracellular ROS levels in prion-treated lymphocytes, predominantly detecting peroxides (*35*). The dichlorofluorescein (DCF) fluorescence from prion treated lymphocytes was monitored under a fluorescence microscope.

Measurement of Intracellular Calcium Influx—$[Ca^{2+}]_i$s were quantified by monitoring the fluorescence ratio of the calcium indicator dye Fura-2 AM. Cells were incubated for 2 h with fibrils as Aβ(1–42) and prion peptides (60 μM each), then washed with PBS solution. The cells were then loaded with 1 μM of the acetoxymethyl ester form of Fura (Fura-2 AM), washed twice and resuspended in HBSS (Hanks' Balanced Salt Solution) containing 1.26 mM $CaCl_2$ at 5×10^6 cells/ml, then used for experiments. Cells were immediately used for calcium influx measurements and $[Ca^{2+}]_i$ was quantified as published (*36*). Fluorescence intensities were obtained using a Cary Bio-50 spectrofluorimeter. The ratio of the fluorescence emission of the cells using two different excitation wavelengths of 340 and 380 nm, at emission wavelength of 510 nm was monitored continuously for 10 min at one second intervals to determine calcium influx.

Peptide Membrane Interaction–Isolation of Lipid Raft—Lymphocyte lipid rafts were isolated as detergent insoluble, low-density materials (DRM) as described earlier (*37*). Briefly, lymphocyte (number of cells = 1×10^6) membranes were disrupted by treatment with Triton X-100, and various lipid microdomains were fused to each other. We isolated a low-density, Triton X-100 insoluble fraction from lymphocyte membranes, after incubation with pyrene-labeled prion fibrils. Pyrene-labeled $A\beta_{1-42}$ fibrils were used as a control. The pyrene label does not significantly alter the solubility and aggregation properties of the peptides (*38*). Fractions were simultaneously recovered from 10% and 30–40% sucrose interfaces, respectively, after sucrose gradient centrifugation of Triton X-100 treated, detergent solublized lymphocytes. It is necessary to remove the lipid raft material for the estimation of prion fragments after Triton X-100 treatment of lymphocyte fractions. The ratios of bound/free pyrene-labeled peptides were quantified by fluorescence spectroscopy. The experiments were also carried out with pyrene-labeled aggregates in the absence of cells, and the aggregates were sedimented by centrifugation at 400,000 × *g* for 4 h in sucrose gradients at 4°C.

RESULTS AND DISCUSSION

The non-specific interaction of peptides with membranes has been reported to trigger patching in lymphocytes, leading to endocytosis (*39–42*). We sought to address whether the surface activity of the prion fragments could be correlated with their lymphocyte toxicity (*40*, *41*). All peptides formed stable Langmuir films at the air-water interface. Plots of the surface pressure as a function of molecular area for Aβ(1–42) and prion peptides are shown in Fig. 1. From the isotherms in Fig. 1, the mean surface area occupied by each protein molecule in the presence and absence of phospholipid was estimated by extrapolating the linear portion of each curve to a surface pressure equal to zero. The molecular surface areas of the peptide film in air-water and air-lipid interfaces are given in Table 1. The films remained stable at surface pressures corresponding to their assembled state ($14 \approx 21$ mNm^{-1} in prion peptides and $27 \approx 29$ mNm^{-1} in Aβ peptide). The areas (30–140 Å^2) of individual peptide molecules in the Langmuir–Blodgett experiments are significantly lower than expected for peptides folded into β-sheets (*30*, *43*, *44*). The packing of the amyloid peptides may preclude hydrophobic regions in the assemblage over the air-water interface (*45*). The structure modeled in Scheme 1 is consistent with the experimental results demonstrating a β-sheet structure and multimeric nature of assembly. The proposed assembly of prion peptides at the air water interface in the absence and presence of a lipid monolayer is shown in Scheme 1. The hydrophobic tail part of the lipid layer holds the oligomeric prion peptide assembly.

Such multimeric aggregate formation is also characteristic of amyloidogenic peptides (*45*, *46*). Interestingly, upon adding the lipid mixture, the surface area of the peptide assemblage is not changed, indicating that the multimeric assembly is not lipid dispersible. Compared to HuPrP (113–127) and HuPrP (119–126), the HuPrP (121–127) peptide film showed a marked increase in collapse pressure indicating that the peptide is more stable in lipid than in non-interacting matrices (Fig. 1d).

Lipid monolayers have proven to be sensitive tools for the study of lipid–peptide and lipid–protein interactions (*47*, *48*). Aβ(1–42) is an amphipathic molecule that is reported to perturb membranes through lipid binding, and to alter cell function (*49*, *50*). The change in area for Aβ(1–42) with time is shown in curve (a) of Fig. 2A. Previous studies showed Aβ(1–42) to exhibit only modest surface activity (*51*). In Fig. 2A, curves (b–d) show the time courses of area increase (Δ*A*) of the three different peptide films formed from HuPrP (113–127), HuPrP (119–126) and HuPrP (121–127), respectively. The addition of HuPrP

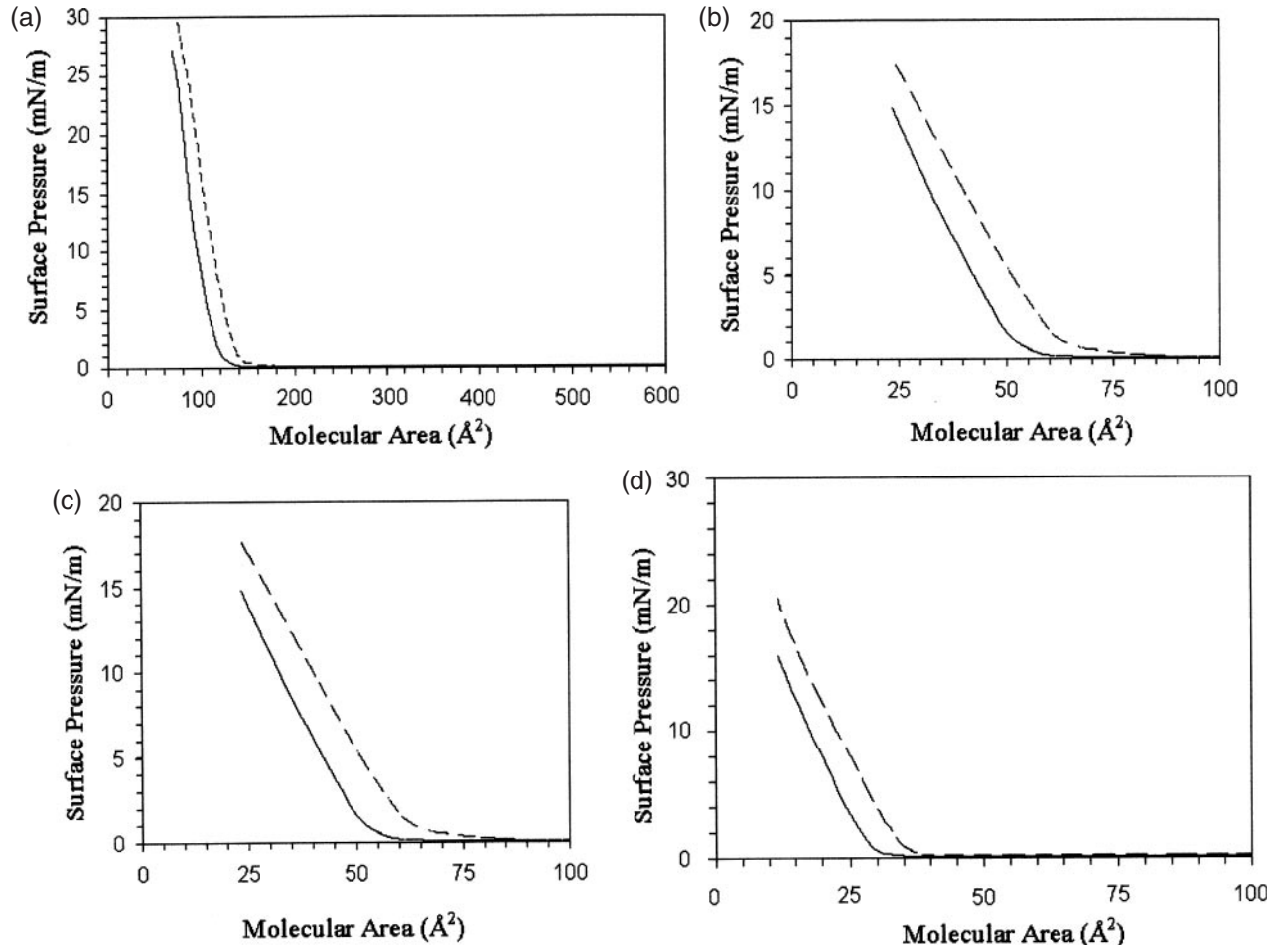

Fig. 1. **Surface behaviour of amyloid peptide monolayers.** Variations in the surface pressure with the mean molecular areas of peptide alone (solid line) and mixed lipid-peptide films at peptide molar fraction (x_p) of 0.5 (broken line), Aβ(1–42) (a), HuPrP (113–127) (b), HuPrP (119–126) (c) and HuPrP (121–127) (d). The subphase was 10% acetonitrile in 10 mM PBS, pH 7.4.

Table 1. Langmuir-Blodgett studies showing mean molecular area and surface pressure of amyloid peptide films.

Peptide	Area in water (Å^2)	Area in lipid (Å^2)	Collapse pressure in water (mN m^{-1})	Collapse pressure in lipid (mN m^{-1})
$A\beta_{1-42}$	121	137	27	29
HuPrP (113–127)	54	65	15	18
HuPrP (119–126)	52	66	14	18
HuPrP (121–127)	29	35	16	21

(113–127) to the sub-phase resulted in an increase in area after 80s, and the difference in area was twice that of HuPrP (121–127). HuPrP (119–126) produced no change in molecular area up to 175 s. For HuPrP (121–127), ΔA increased after 75s. From our earlier observation, it is known that HuPrP (121–127) has the least helical propensity in the soluble form among the prion peptides used in the present investigation (*16*, *17*). These results indicate that there is a negative correlation between the helical conformation of the prion peptides and their ability to bind to phospholipids and their insertion properties. Further, HuPrP (113–127) and HuPrP (121–127) are comparatively more effective in membrane penetration as compared to HuPrP (119–126). The addition of peptides markedly affects the lipid domain organization in time-dependent manner. The surface activities of the different peptides were correlated by plotting of theoretical peptide molecular area versus change in molecular area (ΔA) of the lipid film (Fig. 2B). The linear plot suggests that the surface activity of the peptide on the lipid film is directly proportional to the surface area of the peptide. However among the three-prion peptides, HuPrP (119–126) showed delayed binding to the lipid film. These data suggest that minor sequence changes alter the rate of peptide binding to the membrane surface.

The MTT assay measures the reduction of 3-(4,5-Dimethylthiazol-2yl)-2–5-diphenyltetrazolium bromide (MTT) into an insoluble formazan product by the mitochondria of viable cells (*34*). In our earlier work, we reported the aggregation state of prion peptides. All freshly

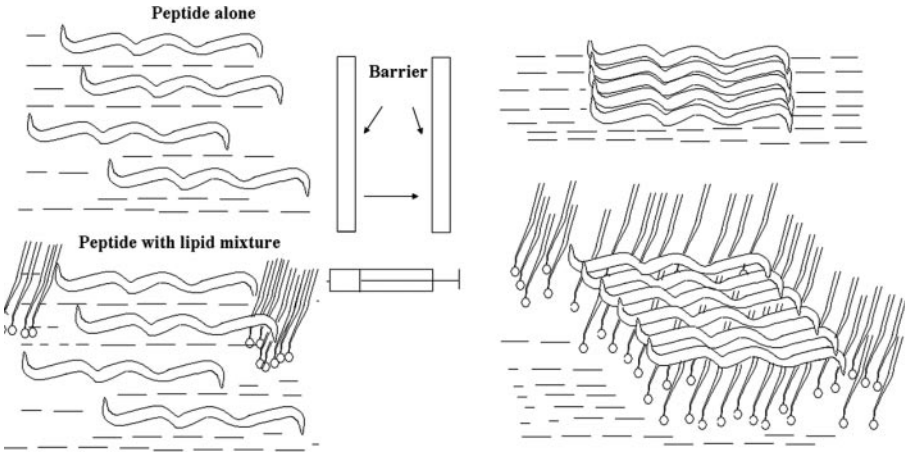

Scheme 1. **Possible model for PrP assembly in the presence and absence of phospholipid films at the air-water interface.**

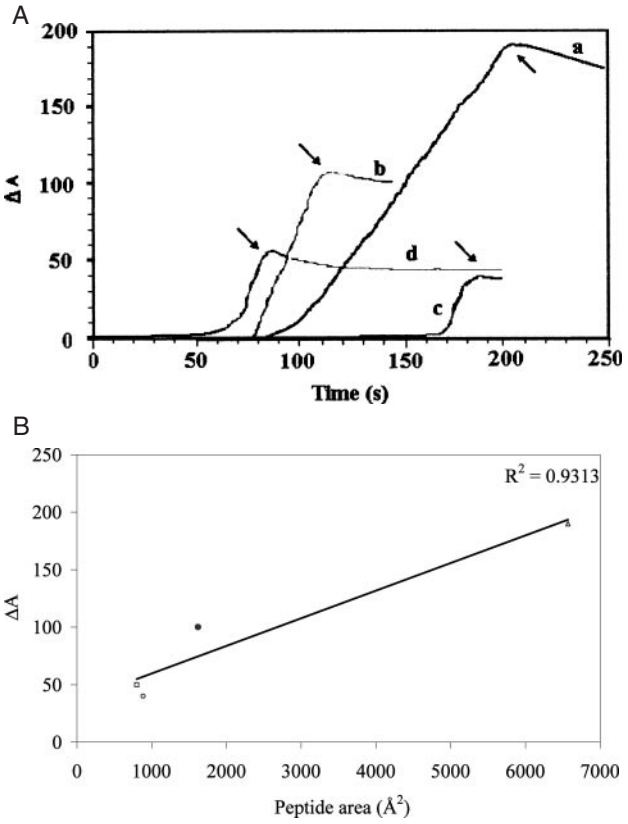

Fig. 2. **A: Membrane penetration of amyloid peptides, A β (1–42) (a), HuPrP (113–127) (b), HuPrP (119–126) (c) and HuPrP (121–127) (d) at a pressure of 21, 17, 20 and 22 mNm^{-1}, respectively.** Arrows indicate the maximum change in the area of the film during penetration. **B: Correlation between peptide area and membrane penetration.** Plot of the area increase in the lipid film upon the addition of peptide *versus* peptide surface area. Peptide areas are indicated as Aβ (1–42) (open triangles), HuPrP (113–127) (solid circles), HuPrP (119–126) (open circles) and HuPrP (121–127) (open squares).

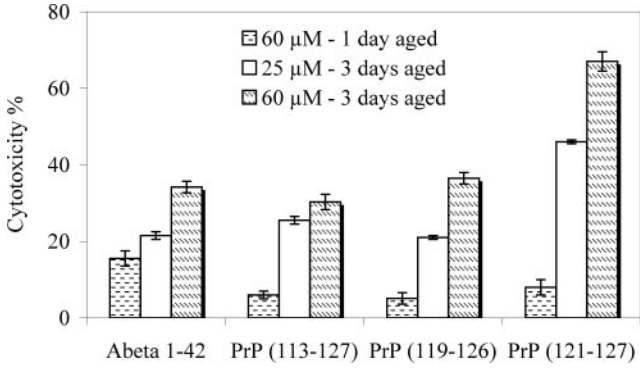

Fig. 3. **Cytotoxic effects of Aβ and prion peptides on lymphocytes assessed by MTT reduction assay.** Cells were treated with one and three days aged Aβ and prion peptides. Data are means ± SD from 4 dishes.

dissolved Prion peptides assumed a random coil conformation in water, and over a period of three days time, the random-coil monomer transformed into β-sheet sheet aggregates, as observed by CD spectroscopy (*15–17*). In the present study, lymphocytes were exposed to freshly solubilised (random-coil), and one and three days (beta-sheet) aged prion peptides. The Aβ(1–42) fibril treated and untreated cells were used as positive and negative controls, respectively. Incubation of lymphocytes with freshly solublised prion peptides showed no toxicity (data not shown). From Fig. 3, it can be inferred that the incubation of lymphocytes with one-day aged prion fragments (60 μM) resulted in no significant cell death. Under our experimental conditions, monomeric HuPrP (113–127), HuPrP (119–126) and HuPrP (121–127) did not significantly affect the lymphocytes as observed by MTT reduction activity. The cellular capacity to reduce MTT was decreased by incubation with fibrillar Aβ(1–42) as shown in Fig 3. Incubation with 25 μM and 60 μM Aβ(1–42) fibrils resulted in 21% and 36% cell death, respectively. Treatment with 25 μM and 60 μM HuPrP (113–127) fibrils resulted in 25% and 30% toxicity, respectively. However, incubation with HuPrP (119–126) and HuPrP (121–127) fibrils resulted in concentration-dependent changes in toxicity. Treatment with 25 and 60 μM HuPrP (119–126) fibrils caused 20% and 40% cytotoxicity ($p < 0.01$). Exposure of lymphocytes to 25 μM and 60 μM HuPrP (121–127) fibrils caused 40% and 60% cell death, respectively ($p < 0.001$). Hope, *et al.* demonstrated that the

ability of PrP (106–126) to form fibrils is important for its toxicity, and that nonfibrillar PrP (106–126) is not neurotoxic (*52*). The results show that the toxicity of the prion fragments is related to their physical state, and that the toxic fibrillar assemblage formed by day three is significantly more toxic than peptides in the monomeric state.

ROS levels were measured in peptide-exposed lymphocytes. Figure 4A shows the time course of peptide induced DCF fluorescence in lymphocytes. The synthetic PrP peptide fibrils produced variations in the ROS levels. Upon incubation with the fibrillar Aβ(1–42) positive control, a five-fold increase in DCF fluorescence was observed, whereas only a one-fold increase in DCF was observed upon incubation with HuPrP (113–127) fibrils. HuPrP (119–126) and HuPrP (121–127) fibrils produced a four-fold increase in fluorescence as compared with the control ($p < 0.001$). Fluorescence microscopic pictures of prion treated lymphocytes are shown in Fig. 4B. The results shown in Fig. 4B reveal that treatment with HuPrP (119–126) and HuPrP (121–127) fibrils significantly increases the DCF fluorescence, indicating an enhancement of reactive oxygen species in lymphocytes. Recently the oxidative oxidative and neurotoxic properties of $A\beta_{25-35}$ were shown using the DCF fluorescence method (*53*). The results in Fig. 4 reveal that the mechanism of the toxicity of HuPrP (119–126) and HuPrP (121–127) fibrils may involve the propagation of oxidative damage.

Figure 5 shows changes in intracellular calcium levels in lymphocytes treated with HuPrP (119–126), HuPrP (121–127), and Aβ(1–42) fibrils. The addition of prion fibrils to Fura-2–loaded lymphocytes induced a fluorescence change characterized by a rapid rise in $[Ca^{2+}]_i$ (600 s), followed by a slower decrease. As shown in Fig. 5, the rise in $[Ca^{2+}]_i$ was dependent on peptide structure. Treatment with HuPrP (113–127) fibrils resulted in a 6% increase in calcium levels over the basal level. However, HuPrP (119–126) fibrils caused an increase in $[Ca^{2+}]_i$ of 14%. HuPrP (121–127) fibrils elevate the calcium level as compared to the basal value (22%) at the lowest effective concentration of any of the fibrils (20 μM, $n = 4$). $A\beta_{1-42}$ fibrils caused a 26.5% increase in the $[Ca^{2+}]_i$ in lymphocytes.These results are in agreement with the findings for astrocytes treated with beta amyloid fragments (*54*). Earlier studies on PrP (106–126)-treated leukocytes showed a similar substantial increase in calcium influx (*13*). The results indicate that the HuPrP (113–127) sequence is ineffective in increasing $[Ca^{2+}]_i$, which remain almost at the basal level. However, the HuPrP (119–126) fibrils caused a moderate increase in $[Ca^{2+}]_i$. The Aβ(1–42) and HuPrP (121–127) fibrils caused a significant increase in the calcium level. One possible explanation involves a disturbance in calcium homeostasis, which depends on a calcium pump. Amyloid peptides are reported to alter intracellular calcium levels either by interaction through intrinsic ion transporting proteins such as calcium channels in the membrane surface, or the activation of the signal transduction cascade through IP_3-modulated calcium channels (*55*). Increased levels of oxidative stress and the disruption of cellular calcium homeostasis are believed to contribute to neuronal dysfunction and degeneration in many age-related neurodegenerative conditions including Alzheimer's disease, Parkinson's disease, Huntington's disease and stroke. It has been reported that in Alzheimer's disease, an accumulation of aggregation prone forms of Aβ(1–42) results in membrane lipid peroxidation (*55*). The destabilization Ca^{2+} homeostasis can also promote free radical production by activating the enzyme nitric oxide synthase (NOS), leading to the production of nitric oxide, a free radical that can interact with superoxide to form the toxic compound peroxynitrite (*55*). An earlier study on the $A\beta_{25-35}$ fragment, which is the cytotoxic sequence of the amyloid peptide, showed it to induce apoptosis in peripheral blood lymphocytes (PBL) representing a remarkable example of a non-neuronal model that can provide insight into the biological processes of response to amyloidogenic fragment-induced oxidative stress by displaying different cell death pathways (*56*). The prion peptide induced modification of Ca^{2+} homeostasis is the result of prion peptide interaction with intrinsic ion transport proteins, *e.g.* L-type Ca^{2+} channels in the surface membrane, and IP3-modulated Ca^{2+} channels in the internal membranes, and/or the formation of cation channels (*13*). These two mechanisms of action lead to changes in Ca^{2+} homeostasis that further augment the abnormal electrical activity and distortion of signal transduction, causing cell death.

The binding to immune receptors by antigenic peptides may lead to activation, cell proliferation, differentiation and effector functions. The initiation and propagation of the signaling events taking place in lymphocytes occur in the lipid raft regions. These domains contain many lipid-modified signaling proteins such as tyrosine kinases of the Src family, GPI (glycosylphosphatidylinositol)-linked proteins as well as adaptor proteins. The confinement of peptide ligands and signaling molecules in membrane subdomains suggests that lipid rafts function as platforms for the formation of multicomponent transduction complexes (*57*, *58*). It should be mentioned that raft sequesterization leads to very high peptide concentrations in the membrane interface. Upon receptor binding, immune receptors become raft-associated and additional components of the signaling pathways are recruited to rafts in order to form signaling complexes.

Recent studies have shown that the access to and translocation of peptides into lipid rafts are developmentally regulated (immature versus mature cells, Th1 *versus* Th2 lymphocytes) and sensitive to extracellular peptide fragments (*59*). To analyze the nature of binding of PrP peptides to membrane microdomains, pyrene-labeled PrP peptides were incubated with lymphocytes. Cells were lysed in buffer containing ice-cold Triton X-100, and the detergent-insoluble complexes were separated by flotation in 10 % to 40 % sucrose gradients. After ultracentrifugation, most PrP molecules were detected in the sucrose fractions containing caveolae-like domains (CLDs), whereas no PrP was found in the lysate fractions, and only minor amounts were recovered from the pellets formed by incompletely solubilized cell debris. The control experiments carried out with pyrene- labeled aggregates in the absence of cells showed complete pelleting of the aggregates from the sucrose gradient. No significant amounts of peptide aggregates were found in the lipid raft fraction.

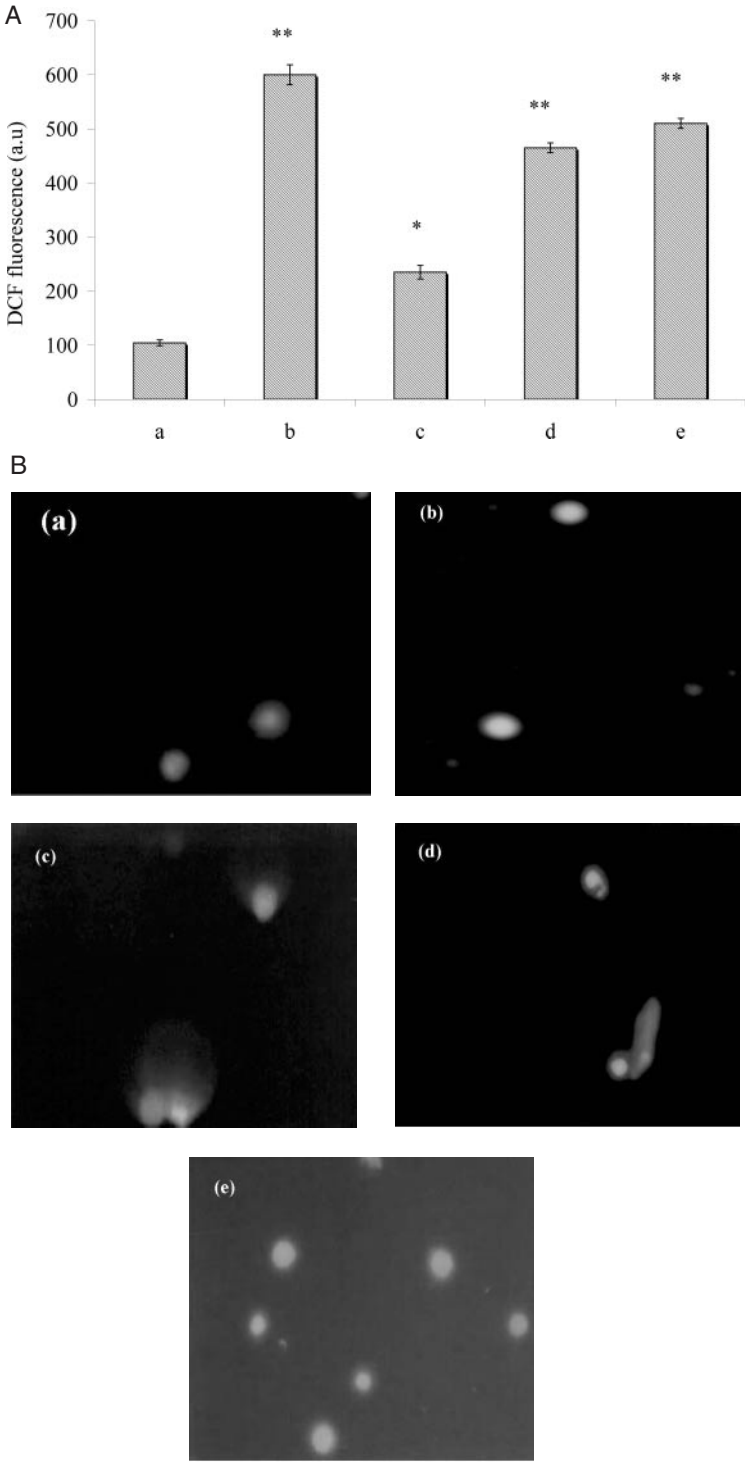

Fig. 4. **A: Production of reaction oxygen species in beta amyloid and prion treated lymphocytes as assessed by DCF fluorescence.** Cells were treated with 25 μM of each peptide. Control (a), Aβ (1–42) (b), HuPrP (113–127) (c), HuPrP (119–126) (d) and HuPrP (121–127) (e). **B: Fluorescence microscopic pictures showing the increase in dichlorofluorescein (DCF) fluorescence during exposure to amyloid peptides.** Lymphocytes control (a), exposed to 25 μM of Aβ(1–42) (b), HuPrP (113–127) (c), HuPrP (119–126) (d), and HuPrP (121–127) (e). Photographs were captured at 30 min time intervals.

The percentage of pyrene labeled peptides in the CLD fractions to that in the Triton X-100 soluble fraction is shown in. Fig 6. It can be seen from the figure that the bound/free ratio of pyrene labeled HuPrP (121–127) fibrils with lipid raft is higher. The results of this study demonstrate that there is a possible involvement of lipid rafts in the cytotoxicity of prion peptides. The identification of pyrene labeled Prion fragments (121–127) in CLDs derived

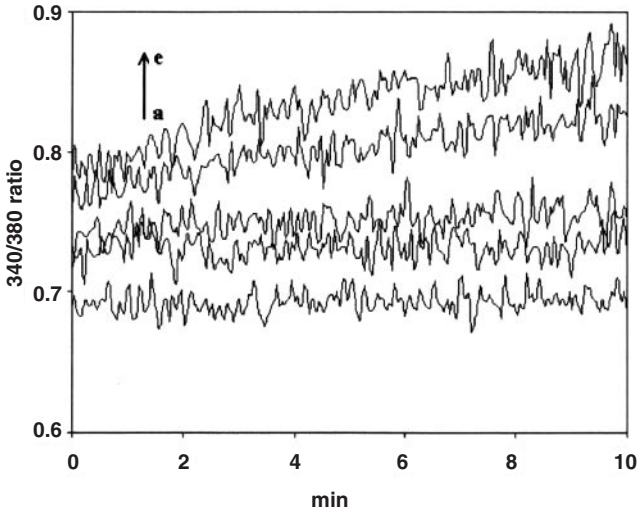

Fig. 5. **Lymphocytes were loaded with Fura 2 as described in "MATERIALS AND METHODS" and resuspended at 5×10^6 cells/ml in HBSS containing 1.26 mM $CaCl_2$.** The Figure shows the $[Ca^{2+}]_i$ rise as increase in fluorescence intensity at excitation 340 nm/380 nm caused by control without peptide (a), HuPrP (113–127) (b), HuPrP(119–126) (c), Aβ(1–42) (d) and HuPrp (121–127) (e) respectively. The peptide concentration was 20 μM.

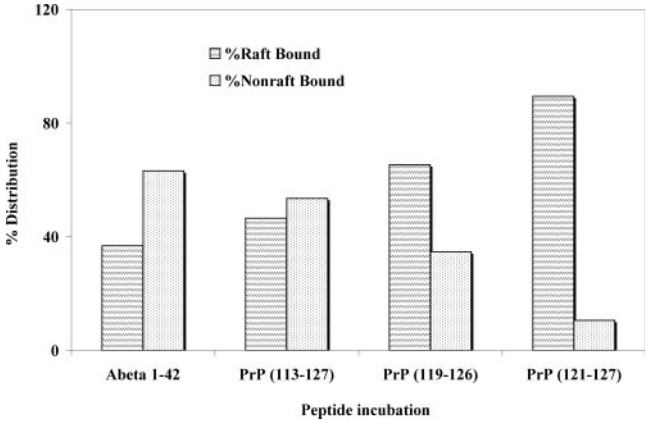

Fig. 6. **Distribution of prion peptides into lipid rafts in lymphocytes.** The ratio of raft bound and nonraft bound amyloid are depicted at labeled pyrene peptide concentration of 10 μM. The values are the averages of three different findings.

from plasma membrane fractions may provide insight into the mode of spread and prion infection through the central nervous system and other organs. An earlier report revealed that the GPI anchor of PrP^{Sc} might facilitate its exchange between cell surfaces, as described for other GPI-anchored proteins (*60*). Lipid rafts have been implicated in numerous cellular processes including signal transduction, membrane trafficking, cell adhesion, and molecular sorting (*61*, *62*). The number of molecules involved in cellular signal processing is enriched in lipid rafts (*62*). Lipid rafts may also serve as docking sites for certain extracellular ligands (*37*, *59*).

In conclusion, the investigation of these prion peptides could enhance our understanding of their structure-function relationships and elucidate the molecular events underlying their interaction with lymphatic cellular membranes. Our studies show PrP fragment assemblage into lymphocytes resulting in cell death, which may explain the role of the proteolytically degraded PrP^{sc} peptide involved in selective lymphatic depletion that is essential for neuroinvasion. We found that short peptide fragments are more toxic and membrane perturbing than larger prion peptides and $A\beta_{1-42}$, indicating the role of smaller peptide in modulating lymphocyte responses. The significant difference between HuPrP (119–126) and HuPrP (121–127) indicate that a mild proteasomal processing frame shift can result in peptides with different lymphocyte toxicities through coordinated events such as oxidative stress, raft sequesterization and calcium ion influx.

We are grateful to Dr. T. Ramasami, Director, CLRI, Chennai, for his support. We thank Mr. K. S. Satheeshkumar for technical help. One of the authors, J. Murali, thanks the Council of Scientific and Industrial Research (CSIR), India, for a Senior Research Fellowship.

REFERENCES

1. Kimberlin, R.H. and Walker, C.A. (1989) Pathogenesis of scrapie in mice after intragastric infection. *Virus. Res* **12**, 213–220
2. Aguzzi, A. (2000) Prion diseases, blood and the immune system: concerns and reality. *Haematologica* **85**, 3–10
3. Jeffrey, M., McGovern, G., Goodsir, C.M., and Bruce, M.E. (2000) Sites of prion protein accumulation in scrapie-infected mouse spleen revealed by immuno-electron microscopy. *J. Pathol.* **191**, 323–332
4. Klein, M.A., Kaeser, P.S., Schwarz, P., Weyd, H., Xenarios, I., Zinkernagel, R.M., Carroll, M.C., Verbeek, J.S., Botto, M., Walport, M.J., Molina, H., Kalinke, U., Acha-Orbea, H., and Aguzzi, A. (2001) Complement facilitates early prion pathogenesis. *Nat. Med.* **7**, 488–492
5. Caughey, B. and Lansbury, P.T. (2003). Protofibrils, pores, fibrils, and neurodegeneration: separating the responsible protein aggregates from the innocent bystanders. *Annu. Rev. Neurosci.* **26**, 267–298
6. Luhr, M.K., Wallin, R.P.A., Ljunggren, H., Löw, P., Taraboulos, A., and Kristensson, K. (2002) Processing and degradation of exogenous prion protein by CD11c(+) myeloid dendritic cells in vitro. *J. Virol.* **76**, 12259–12264
7. Enari, M., Flechsig, E., and Weissmann, C. (2001) Scrapie prion protein accumulation by scrapie-infected neuroblastoma cells abrogated by exposure to a prion protein antibody. *Proc. Natl. Acad. Sci. USA* **98**, 9295–9299
8. Peretz, D., Williamson, R.A., Kaneko, K., Vergara, J., Leclerc, E., Schmitt-Ulms, G., Mehlhorn, I.R., Legname, G., Wormald, M.R., Rudd, P.M., Dwek, R.A., Burton, D.R., and Prusiner, S.B. (2001) Antibodies inhibit prion propagation and clear cell cultures of prion infectivity. *Nature* **412**, 739–743
9. Beringue, V., Demoy, M., Lasmezas, C.I., Gouritin, B., Weingarten, C., Deslys, J.P., Andreux, J.P., Couvreur, P., and Dormont, D. (2000) Role of spleen macrophages in the clearance of scrapie agent early in pathogenesis. *J. Pathol.* **190**, 495–502
10. Carp, R.I. and Callahan, S.M. (1981) In vitro interaction of scrapie agent and mouse peritoneal macrophages. *Intervirology* **16**, 8–13
11. Souan, L., Tal, Y., Felling, Y., Cohen, I.R., Taraboulos, A., and Mor, F. (2001) Modulation of proteinase-K resistant prion protein by prion peptide immunization. *Eur. J. Immunol.* **31**, 2338–2346

12. Le, Y., Yazawa, H., Gong, W., Yu, Z., Ferrans, V.J., Murphy, P.M., and Wang, J.M. (2001) The neurotoxic prion peptide fragment PrP(106–126) is a chemotactic agonist for the G protein-coupled receptor formyl peptide receptor-like 1. *J. Immunol.* **166**, 1448–1451
13. Diomede, L., Sozzani, S., Luini, W., Algeri, M., De Gioia, L., Chiesa, R., Lievens, P.M., Bugiani, O., Forloni, G., Tagliavini, F., and Salmona, M. (1996) Activation effects of a prion protein fragment [PrP-(106–126)] on human leucocytes. *Biochem. J.* **320**, 563–570
14. Glatzel, M. and Aguzzi, A. (2001) The shifting biology of prions. *Brain. Res. Brain. Res. Rev.* **36**, 241–248
15. Satheeshkumar, K.S. and Jayakumar, R. (2002) Sonication induced sheet formation at the air-water interface. *Chem. Commun.(Camb)* **19**, 2244–2245
16. Satheeshkumar, K.S. and Jayakumar, R., (2003) Conformational polymorphism of the amyloidogenic peptide homologous to residues 113–127 of the prion protein. *Biophys. J.* **85**, 473–483
17. Satheeshkumar, K.S., Murali, J., and Jayakumar, R. (2004) Assemblages of prion fragments: novel model systems for understanding amyloid toxicity. *J. Struct. Biol.* **148**, 176–193
18. Yoshida, H., Matsushima, N., Kumaki, Y., Nakata, M., and Hikichi, K. (2000) NMR studies of model peptides of PHGGGWGQ repeats within the N-terminus of prion proteins: a loop conformation with histidine and tryptophan in close proximity. *J. Biochem.* **128**, 271–281
19. Forloni, G., Del Bo, R., Angeretti, N., Chiesa, R., Smiroldo, S., Doni, R., Ghibaudi, E., Salmona, M., Porro, M., Verga, L., Giaccone, G., Bugiani, O., and Tagliavini, F. (1994) A neurotoxic prion protein fragment induces rat astroglial proliferation and hypertrophy. *Eur. J. Neurosci.* **6**, 1415–1422
20. Selvaggini, C.L., De Gioia, L., Cantu, E., Ghibaudi, L., Diomde, F., Passerini, G., Forloni, G., Bugiani, O., Tagliavini, F., and Salmona, M. (1993) Molecular characteristics of a protease-resistant, amyloidogenic and neurotoxic peptide homologous to residues 106–126 of the prion protein. *Biochem. Biophys. Research. Commun.* **194**, 1380–1386
21. De Gioia, L., Selvaggini, C., Ghibaudi, E., Diomede, L., Bugiani, O., Forloni, G., Tagliavini, F., and Salmona, M. (1994) Conformational polymorphism of the amyloidogenic and neurotoxic peptide homologous to residues 106–126 of the prion protein. *J. Biol. Chem.* **269**, 7859–7862
22. Brown, D.R., Wong, B.S., Hafiz, F., Clive, C., Haswell, S. J., and Jones, I.M. (1999) Normal prion protein has an activity like that of superoxide dismutase. *Biochem. J.* **344**, 1–5
23. Ettaiche, M., Pichot, R., Vincent, J.P., and Chabry, J. (2000) In vivo cytotoxicity of the prion protein fragment 106–126. *J. Biol. Chem.* **275**, 36487–36490
24. Legname, G., Baskakov, I.V., Nguyen, H.O., Riesner, D., Cohen, F.E., DeArmond, S.J., and Prusiner, S.B. (2004) Synthetic mammalian prions. *Science* **305**, 673–676
25. McHattie, S.J., Brown, D.R., and Bird, M.M. (1999) Cellular uptake of the prion protein fragment PrP106–126 in vitro. *J. Neurocytol.* **2**, 149–159
26. Leucht, C., Simoneau, S., Rey, C., Vana, K., Rieger, R., Lasmezas, C.I., and Weiss, S. (2003) The 37 kDa/67 kDa laminin receptor is required for PrP(Sc) propagation in scrapie-infected neuronal cells. *EMBO Rep.* **3**, 290–295
27. Bate, C., Langeveld, J., and Williams, A. (2004) Manipulation of PrPres production in scrapie-infected neuroblastoma cells. *J. Neurosci. Methods* **138**, 217–223
28. Herms, J.W., Madlung, A., Brown, D.R., and Kretzschmar, H.A. (1997) Increase of intracellular free Ca2+ in microglia activated by prion protein fragment. *Glia* **2**, 253–257
29. Bodanszky, M. and Bodanszky, A. (eds.) (1984) *The Practice of Peptide Synthesis*, Springer-Verlag, Berlin, Heidelberg, New York, Tokyo
30. Maget-Dana, R. (1999) The monolayer technique: a potent tool for studying the interfacial properties of antimicrobial and membrane-lytic peptides and their interactions with lipid membranes. *Biochim. Biophys. Acta* **1462**, 109–140
31. Gaines, G.L. (1966) *Insoluble Monolayers at Liquid–Gas Interfaces* (Prigogine, ed.) Interscience, New York
32. Fidelio, G.D., Maggio, B., Cumar, F.A., and Caputto, R. (1981) Interaction of glycosphingolipids with melittin and myelin basis protein in monolayers. *Biochem. J.* **193**, 643–646
33. Jayakumar, R., Murali, J., Koteeswari, D., and Gomathi, K. (2004) Cytotoxic and membrane perturbation effects of a novel amyloid forming model peptide poly(leucine-glutamic acid). *J. Biochem.* **136**, 457–462
34. Hansen, M.B., Nielsen, S.E., and Berg, K. (1989) Re-examination and further development of a precise and rapid dye method for measuring cell growth/cell kill. *J. Immunol. Methods* **119**, 203–210
35. Nakamura, K., Fushimi, K., Kouchi, H., Mihara, K., Miyazaki, M., Ohe, T., and Namba, M. (1998) Inhibitory effects of antioxidants on neonatal rat cardiac myocyte hypertrophy induced by tumor necrosis factor-alpha and angiotensin II. *Circulation* **98**, 794–799
36. Lukyanetz, E. A., Stanika, R. I., Koval, L. M., and Kostyuk, P. G. (2003) Intracellular mechanisms of hypoxia-induced calcium increase in rat sensory neurons. *Arch. Biochem. Biophys.* **410**, 212–221
37. Brown, D.A. and London, E. (2000) Structure and function of sphingolipid- and cholesterol-rich membrane rafts. *J. Biol. Chem.* **275**, 17221–17224
38. Tcherkasskaya, O., Sanders, W., Chynwat, V., Davidson, E.A., and Orser C.S., (2003) The role of hydrophobic interactions in amyloidogenesis: example of prion-related polypeptides. *J. Biomol. Struct. Dyn.* **21**, 353–365
39. Xavier, R., Brennan, T., Li, Q., McCormack, C., and Seed, B. (1998) Membrane compartmentation is required for efficient T cell activation. *Immunity* **8**, 723–732
40. Lahdo, R. and Bessueille, L. (2004) Insertion of the amyloid precursor protein into lipid monolayers: effects of cholesterol and apolipoprotein E. *Biochem. J.* **382**, 987–994
41. Peterson, I.R. and Kenn, R.M. (1994) Equivalence between Two-dimensional and Three-dimensional Phases of Aliphatic Chain Derivatives. *Langmuir* **10**, 4645–4650
42. Yong, W., Lomakin, A., Kirkitadze, M.D., Teplow, D.B., Chen, S.H., and Benedek, G.B. (2002) Structure determination of micelle-like intermediates in amyloid beta -protein fibril assembly by using small angle neutron scattering. *Proc. Natl. Acad. Sci. USA* **99**, 150–154
43. Powers, E.T., Yang, S.I., Lieber, C.M., and Kelly, J.W. (2002) Ordered Langmuir-Blodgett films of amphiphilic beta-hairpin peptides imaged by atomic force microscopy. *Angew. Chem. Int. Ed. Engl.* **41**, 127–130
44. Xu, G., Wang, W., Groves, J.T., and Hecht, M.H. (2001) Self-assembled monolayers from a designed combinatorial library of de novo beta-sheet proteins. *Proc. Natl. Acad. Sci. USA* **98**, 3652–17227
45. Os-Garci'a, V.M.B., Mas-Oliva, J., Ramos, S., and Castillo, R. (1999) Phase transitions in monolayers of human apolipoprotein C1. *J. Phys. Chem. B* **103**, 6236–6242
46. Schladitz, C., Vieira, E.P., Hermel, H., and Mohwald, H. (1999) Amyloid-beta-sheet formation at the air-water interface. *Biophys. J.* **77**, 3305–3310
47. Terzi, E., Holzemann, G., and Seelig, J. (1995) Self-association of beta-amyloid peptide (1–40) in solution and binding to lipid membranes. *J. Mol. Biol.* **252**, 633–642
48. Hanakam, F., Gerisch, G., Lotz, S., Alt, T., and Seelig, A. (1996) Binding of hisactophilin I and II to lipid membranes is controlled by a pH-dependent myristoyl-histidine switch. *Biochemistry* **35**, 11036–11044
49. Wood, W.G., Eckert, G.P., Igbavboa, U., and Müller, W.E. (2003) Amyloid beta-protein interactions with membranes

and cholesterol: causes or casualties of Alzheimer's disease. *Biochim. Biophys. Acta* **1610**, 281–290
50. Bokvist, M., Lindström, F., Watts, A., and Gröbner, G. (2004) Two types of Alzheimer's beta-amyloid (1–40) peptide membrane interactions: aggregation preventing transmembrane anchoring versus accelerated surface fibril formation. *J. Mol. Biol.* **335**, 1039–1049
51. Soreghan, B., Kosmoski, J., and Glabe, C. (1994) Surfactant properties of Alzheimer's A beta peptides and the mechanism of amyloid aggregation. *J. Biol. Chem.* **269**, 28551–28554
52. Hope, J., Shearman, M.S., Baxter, H.C., Chong, A., Kelly, S.M., and Price, N.C. (1996) Cytotoxicity of prion protein peptide (PrP106–126) differs in mechanism from the cytotoxic activity of the Alzheimer's disease amyloid peptide, A beta 25–35. *Neurodegeneration* **5**, 1–11
53. Andersen, J.M., Myhre, O., Aarnes, H., Vestad, T.A., and Fonnum, F. (2003) Identification of the hydroxyl radical and other reactive oxygen species in human neutrophil granulocytes exposed to a fragment of the amyloid beta peptide. *Free Radic. Res.* **37**, 269–279
54. Stix, B. and Reiser, G. (1998) Beta-amyloid peptide 25–35 regulates basal and hormone-stimulated Ca^{2+} levels in cultured rat astrocytes. *Neurosci. Lett*. **243**, 121–124
55. Mattson, M.P., Begley, J.G., Mark, R.J., and Furukawa, K. (1997) Aβ25–35 induces rapid lysis of red blood cells: contrast with Aβ1–42 and examination of underlying mechanisms. *Brain Res* **771**, 147–153
56. Yankner, B.A., Duffy, L.K., and Kirschner, D.A. (1990) Neurotrophic and neurotoxic effects of amyloid beta protein: reversal by tachykinin neuropeptides. *Science* **250**, 279–282
57. Baron, G.S. and Caughey, B. (2003) Effect of glycosyl phosphatidyl inositol anchor-dependent and -independent prion protein association with model raft membranes on conversion to the protease-resistant isoform. *J. Biol. Chem.* **278**, 14883–14892
58. Caughey, B. and Baron, G.S. (2002) Factors affecting interactions between prion protein isoforms. *Biochem. Soc. Trans.* **30**, 565–569
59. Bi, K., Tanaka, Y., Coudronniere, N., Sugie, K., Hong, S., Van Stipdonk, M.J., and Altman, A. (2001) Antigen-induced translocation of PKC-theta to membrane rafts is required for T cell activation. *Nat. Immunol.* **2**, 556–563
60. Baron, G.S., Wehrly, K., Dorward, D.W., Chesebro, B., and Caughey, B. (2002) Conversion of raft associated prion protein to the protease-resistant state requires insertion of PrP-res (PrP(Sc) into contiguous membranes. *EMBO. J.* **21**, 1031–1040
61. Harder, T., Scheiffele, P., Verkade, P., and Simons, K. (1998) Lipid domain structure of the plasma membrane revealed by patching of membrane components. *J. Cell. Biol.* **141**, 929–942
62. Dermine, J.F., Duclos, S., Garin, J., St-Louis, F., Rea, S., Parton, R.G., and Desjardins, M. (2001) Flotillin-1-enriched lipid raft domains accumulate on maturing phagosomes. *J. Biol. Chem.* **276**, 18507–18512